18th Brazilian Congress of Thermal Sciences and Engineering
November 16-20, 2020 (online)

ENC-2020-0433
CHARACTERIZATION OF A COUPLED COPPER-WATER HEAT PIPE WITH A FREE PISTON STIRLING ENGINE

Ana Carolina dos Santos
Instituto Tecnológico de Aeronáutica – ITA
Praça Marechal Eduardo Gomes, 50, 12228-900 Vila das Acacias, SP, Brazil
anna.carolsantos21@gmail.com

Lamartine Nogueira Frutuoso Guimarães
Instituto de Estudos Avançados – IEAv, Divisão de Energia Nuclear
Trevo Coronel Aviador José Alberto Albano do Amarante, 01, 12228-001, São José dos Campos, SP, Brazil
lamar.guima@gmail.com

Valéria Serrano Faillace Oliveira Leite
Instituto de Estudos Avançados – IEAv, Divisão de Suporte Tecnológico
Trevo Coronel Aviador José Alberto Albano do Amarante, 01, 12228-001, São José dos Campos, SP, Brazil
valeria@ieav.cta.br

Rafael Theodoro
Instituto Tecnológico de Aeronáutica – ITA
Praça Marechal Eduardo Gomes, 50, 12228-900 Vila das Acacias, SP, Brazil
rafael_theodor@hotmail.com

Abstract.

Heat pipes are very efficient and passive heat conduction devices. Lately, there have been quite a few studies addressing this application when coupled with a Stirling engine. As for instance, all the research related to the DUFF reactor, the KRUSTY reactor and the KILOPOWER reactor, all from NASA. Interesting to observe, in all those cases each system is quite specific with its application. At the Institute for Advanced Studies (IEAv) there is a great interest in such a study because of the development of its own heat pipe and Stirling engine. Thus, the objective of this work is to experimentally characterize a water-copper heat pipe transporting heat from a thermal source to the hot end of a Stirling engine, both built at IEAv. For this, it is necessary to couple the heat pipe condenser temperature with the Stirling engine hot side temperature. A heat adapter model was developed to connect the heat pipe to the engine's hot side. Experimental tests were realized with copper-water heat pipe with a Wick structure made of brass screen, operating in the temperature range of 20ºC to 285 ºC. With these temperature values, the operating limits, critical pressure, Reynolds number, thermal resistances and thermal power were numerically calculated. This paper characterizes and adapt a heat pipe to transport heat from a conventional thermal source (eventually it will be nuclear) to the hot base of the Stirling engine developed at the IEAv.

Keywords: *Heat pipe, thermosyphon, Stirling engine, heat transfer*

1. INTRODUCTION

One of the biggest challenges in space exploration is producing energy. In this context, the TERRA project conducted by the Institute for Advanced Studies - IEAv develops systems and technologies for power generation in space. Also, these technologies may be used on Earth remote locations. One of these technologies is the Stirling engine. The Stirling engine is a thermal machine that converts heat into electrical energy. The heat may be generated by different energy source, such as: solar, fossil and nuclear (best suited for space and remote locations). The use of a nuclear source requires to shield the Stirling from the neutron radiation. Therefore, it is necessary to use an intermediary device that transfers heat from the nuclear source to the engine and the heat pipe is such one of these devices. It is a passive, two-phase flow sealed device, which rapidly transports large amount of heat with minimal temperature drop.

Figure 1 shows a heat pipe in a horizontal position. The pipe is composed of three concentric layers: the metallic envelope, the wick and the working fluid. The device is also axially divided into three regions: the evaporator, the adiabatic and the condenser (REAY, 2006). In the evaporator region, heat is absorbed from a thermal source and

transferred to the working fluid causing it to change from liquid to vapor. The increase in vapor pressure in the evaporator causes the vapor to leave the evaporator to the condenser, passing through the adiabatic region, carrying the latent heat of vaporization. In the condenser, the vapor releases its latent heat by condensing. The condensed liquid returns to the evaporator through the capillary structure of the wick, by capillary pressure action (heat pipe) or by gravity action (thermosyphon). The pressure inside the heat pipe is equal to the saturation pressure of the working fluid at the operating temperature. The phase change and the biphasic flow circulation continue as long as the temperature gradient between the evaporator and the condenser is maintained (ZOHURI, 2016).

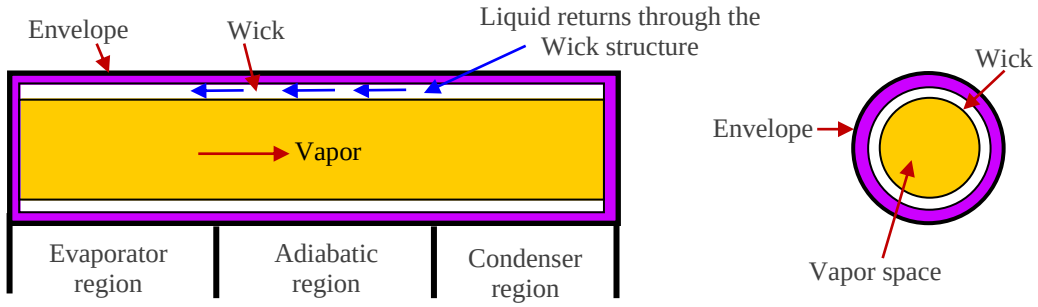

Figure 1. Scheam representation of a heat pipe.

Many mechanisms are capable of limiting the heat transport of a heat pipe. The main limitations are shown in Tab.1.

Table 1. Factors influencing the performance of heat pipes (ZOHURI, 2016).

	Definition	**Causes**	**Possible solutions**
Viscous limit	Viscous forces prevent the flow of vapor in the pipe.	This occurs when the operating temperature is below the recommended temperature.	The operating temperature must be increased.
Sonic limit	The vapor flow reaches sonic speed as it exits the evaporator, resulting in large temperature gradient.	It occurs due to the energy / temperature combination, that is, a lot of energy at low operating temperature. This is usually just a problem at startup.	The flow inserted into the pipe must be reduced.
Entrainment limit	The flow of high speed vapor prevents the condensate from returning to the evaporator. Drying of the fluid inside the pipe may occur.	It occurs when the operating temperature is above the projected temperature or at a very low operating temperature.	The diameter of the vapor space or the operating temperature must be increased.
Boiling Limit	Boiling occurs in the wick which prevents liquid return (drying of heat pipe) with great thermal resistance.	High radial heat flux into the heat pipe evaporator.	Wick structure with a greater heat flow capacity should be used or the applied radial flow should be reduced.
Capillary limit	The capillary action of the wick structure cannot overcome gravitational, liquid, and vapor flow pressure drops.	Power input is too high. Wick structure is not designed appropriately for power and orientation.	Modify the design of wick structure or reduce energy input
Fluid volume filled	The fluid volume filled is the relationship between fluid volume and evaporator volume.	An insufficient amount of fluid causes drying, while an excessive amount combined with high heat flow causes the boiling limit.	For thermosyphon it is recommended to use 60% - 80% (ESDU, 2005) and for heat pipes 100% (KRAMBECK, 2018)

NASA is developing the KILOPOWER system, shown in Fig. 2. The KILOPOWER operates in the 1 to 10 kWe range. It uses alkali metal heat pipes to supply heat to Stirling convertors to produce electricity. And it uses also titanium water heat pipes to remove the waste heat and transport it to the radiators, to be rejected to space (LEE, 2018).

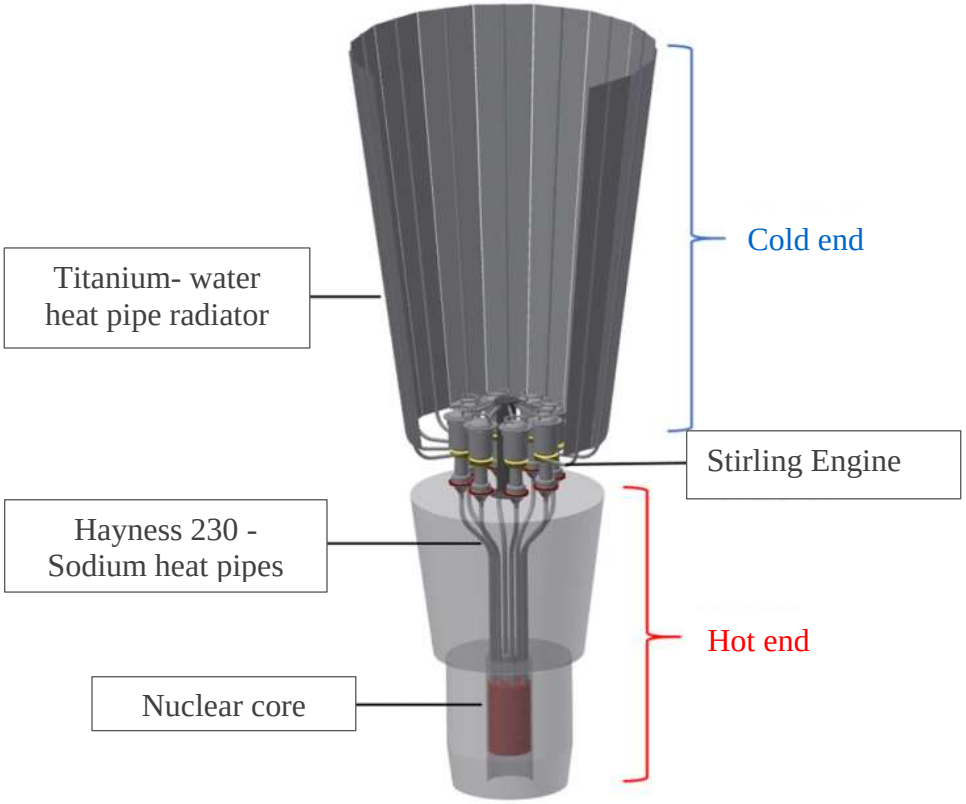

Figure 2. Kilopower System (LEE, 2018).

The application of heat pipes in Stirling engines is poorly studied around the world. The IEAv developed a Free Piston Stirling Engine prototype (SANTOS, 2019), a water/copper heat pipe prototype (EUPHRASIO, 2019) and water/copper thermosyphon prototype (EUPHRASIO, 2016). Those developments may be coupled together. Thus, the objective of this paper is to experimentally characterize a water-copper heat pipe operating in the temperature range sufficient to carry heat from a thermal source to the hot end of a Stirling engine, as shown in Fig. 3 schematic drawing.

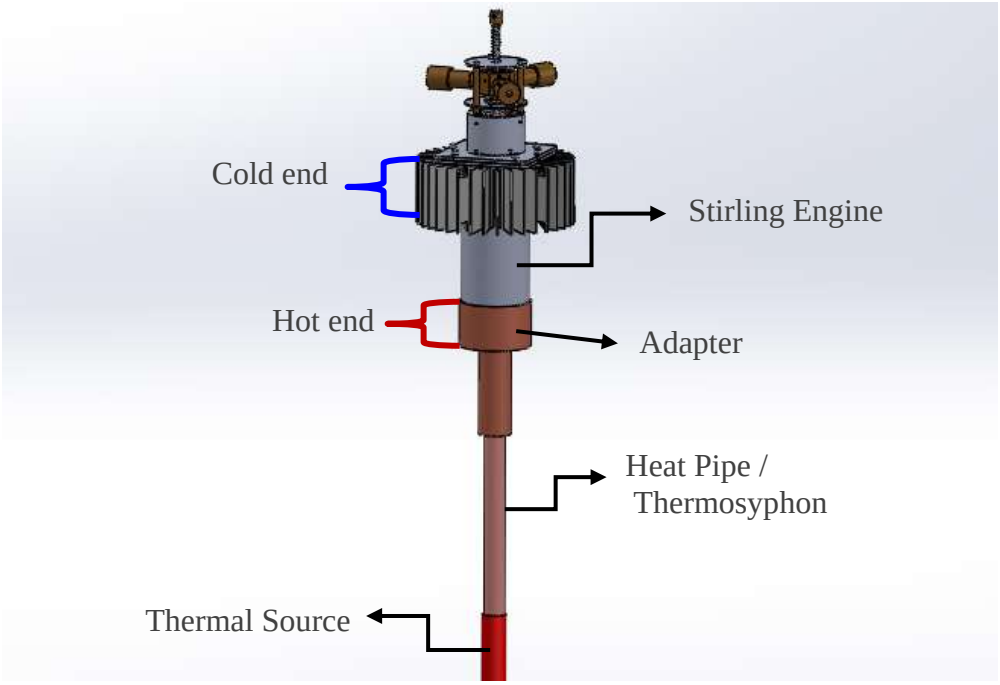

Figure 3. Schematic drawing of the assembly (heat pipe + Stirling engine).

2. METHODOLOGY

2.1. Stirling engine data

Temperatures at the hot and cold ends of the Stirling engine were collected using a Benetech GM900 digital thermometer (Instrument uncertainty ± 2 ºC). The temperatures were collected in the steady state regime at laboratory temperature 22ºC ± 2.5ºC. A device was designed to couple the heat pipe to the engine. The design of this device was done using the commercial software Solidworks and the temperature distribution along the adapter was simulated with the software "*Ansys Transient Thermal.*"

2.2. Characteristics of heat pipe and thermosyphon

Heating conduction experiments were carried out with a heat pipe and a thermosyphon. Both devices were made of copper and use water as working fluid. Figure 4 shows the internal detail of the 100 mesh heat pipe manufactured by EUPHRASIO, 2019.

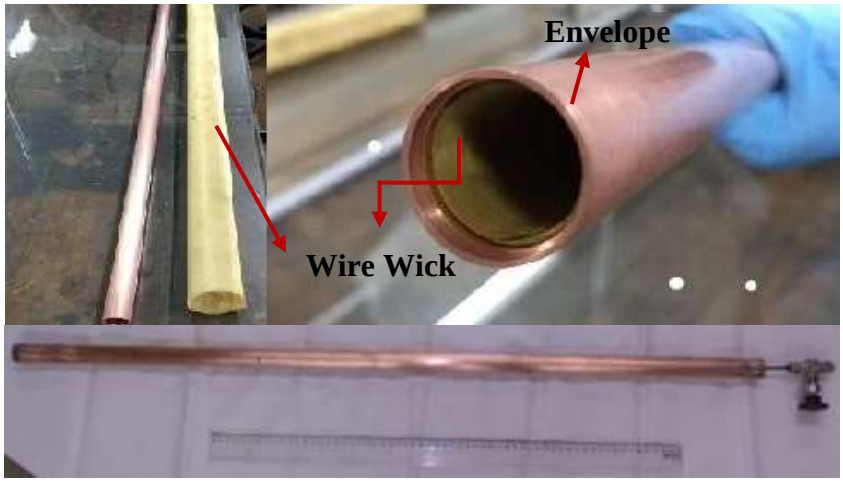

Figure 4. Internal detail of the heat pipe manufactured (EUPHRASIO, 2019).

The dimension specifications of heat pipe and a thermosyphon are presented in Tab.2.

Table 2. Main characteristics of heat pipe (EUPHRASIO, 2019) and thermosyphon (EUPHRASIO, 2016).

Properties	Heat pipe Mesh 100	Thermosyphon
De- External diameter	0.0256 m	0.0256 m
Di - Inner diameter	0.0226 m	0.0226 m
L - Total length	0.9600 m	1.0000 m
FP- Fluid volume filled	50%	50%
Le- Evaporator length = Lc - Condenser length	0.2000 m	0.2000 m
Screen mesh wick	Brass Mesh 100	-

2.3. Experimental Apparatus

Seven T-IOPE thermocouples calibrated for temperatures range between 20 ºC and 300 ºC (Instrument uncertainty ± 0.92 ºC and coverage factor, k = 2). The T-IOPE thermocouples were connected to the predetermined pipe positions are shown in Fig. 5. The NI PXIe-1082 chassis was used to temperature data collection. The software used to collect pipe temperatures was developed in Labview by (EUPHRÁSIO, 2019).

The adiabatic region was isolated using felt (5 cm thickness and thermal conductivity of 0.04 W/m K). Both the pipe and the thermosyphon were fixed upright on a support for the operation of the pipe and for the temperature acquisition. The evaporator was heated using a thermal ribbon (220V).

The pipe temperatures were collected from the moment of thermal ribbon turn on until steady state reach. With these temperature values, averages in each region (condenser, adiabatic and evaporator) were calculated for better visualization of the data in the graphs. Experimental uncertainties are associated with the temperature sensors (T-type thermocouples). To determine the experimental uncertainties of the collected data temperatures, the Error Propagation method described by (HOLMAN, 2011) was used.

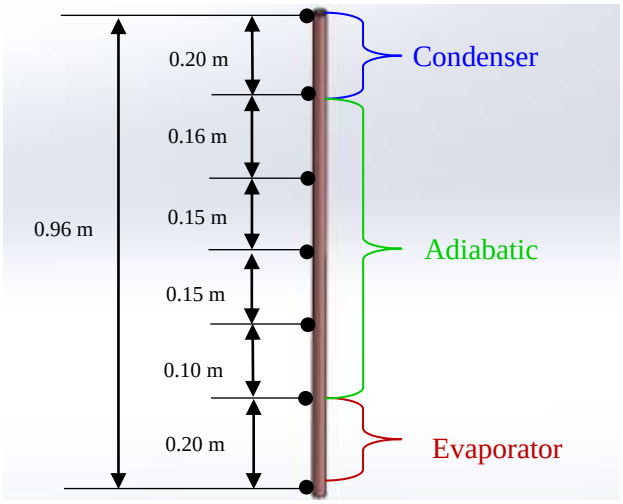

Figure 5. Position of type T thermocouples on the thermosyphon and heat pipe.

With the temperatures collected, it was calculated the Reynolds number, with Eq.1, viscous limit, with Eq.2, sonic limit, with Eq. 3, boiling limit, with Eq. 4, global thermal resistance, with Eq. 5 and the thermal power, with Eq. 6 (ZOHIRI, 2016) and (REAY, 2006). To perform these calculations an Excel program was developed.

$$Re_v = 4 \cdot \frac{q}{\pi \cdot D_i \cdot \mu_v \cdot h_{lv}} \tag{1}$$

$$qmáx_{viscoso} = \frac{{d_v}^2 \cdot h_{lv} \cdot \rho_v \cdot p_v}{64 \cdot \mu_v \cdot L_{eff}} \tag{2}$$

$$qmáx_{sonico} = 0{,}474 \cdot h_{lv} \cdot A_v \cdot \sqrt{\rho_v \cdot p_v} \tag{3}$$

$$q_{ebulição} = \left(\frac{2\pi \cdot L_e \cdot k_{eff} \cdot T_v}{h_{lv} \cdot \rho_v \cdot \ln\left(\frac{D_i}{D_v}\right)} \right) \cdot \left(\frac{2\sigma}{r_n} - P_c \right) \tag{4}$$

$$R = \frac{1}{\mathrm{h}_e \cdot A_e} + \left(\frac{2 \cdot \left[ln\left(\frac{D_e}{Di}\right) + ln\left(\frac{D_i}{Dv}\right) \right]}{2 \cdot \pi \left[l_e \cdot k_{copper} + l_e \cdot k_{eff} + l_c \cdot k_{eff} + l_c \cdot k_{cooper} \right]} \right) + \frac{1}{\mathrm{h}_c \cdot A_c} \tag{5}$$

$$q = \frac{\Delta \mathrm{T}}{\mathrm{R}} = \frac{\mathrm{T_e} - \mathrm{T_c}}{\mathrm{R}} \tag{6}$$

Where k_{eff} is obtained by the Eq. 7.

$$k_{eff} = \frac{k_l \cdot [(k_l + k_w) - (1 - \varepsilon)(k_l - k_w)]}{[(k_l + k_w) + (1 - \varepsilon)(k_l - k_w)]} \tag{7}$$

A_c , A_e and L_{eff} are obtained by the Eq. 8, Eq. 9 and Eq. 10 respectively.

$$\mathrm{A_c} = \pi \cdot D_e \cdot \mathrm{L_c} \tag{8}$$

$$\mathrm{A_e} = \pi \cdot D_e \cdot \mathrm{L_e} \tag{9}$$

$$L_{eff} = \frac{(l_e + l_c)}{2} + l_a \tag{10}$$

The internal circumferential and longitudinal pressures of the pipe can be obtained by Eq. 11 and Eq. 12, respectively.

$$P = \frac{S \cdot (D_e - D_i)}{[D_i + 0.6 \cdot (D_e - D_i)]} \tag{11}$$

$$P = \frac{2 \cdot S \cdot (D_e - D_i)}{[D_i - 0.4 \cdot (D_e - D_i)]} \tag{12}$$

Nomenclature and unit of the equation symbols are shown in the Tab.3.

Table 3. Nomenclature and unit of the equation symbols.

Symbol	Nomenclature	Unit
Re_v	Vapour Phase Reynolds number	
q	Heat flow rate	W
R	Thermal resistance	ºC/W
D_i	Inner diameter	m
D_e	External diameter	m
D_v	Vapour diameter	m
T_e	Evaporator wall temperature	K
T_c	Condenser wall temperature	K
T_v	Vapour temperature	K
ρ_v	Vapour density	Kg/m³
p_v	Vapour pressure	Pa
μ_v	dynamic viscosity	Kg /m.s
h_{lv}	latent heat of vaporization	J/kg
σ	Superficial tension	N/m
L_{eff}	Effective tube length	m
L_e	Evaporator length	m
L_c	Condenser length	m
L_a	Adiabatic length	m
A_v	Cross sectional area of vapour diameter	m²
A_e	Evaporator lateral area	m²
A_c	Condenser lateral area	m²
h_e	Evaporator external convection coefficient	W/m² K
h_c	Condenser external convection coefficient	W/m² K
k_{cooper}	Thermal conductivity of Envelope material	W/m K
k_{eff}	Effective thermal conductivity	W/m K
k_l	Thermal conductivity of the working fluid	W/m K
k_w	Thermal conductivity of wick material	W/m K
ε	Mesh porosity	
r_n	Nucleation radius ($2{,}54 \times 10^{-6}$ m is assumed)	m
P	Internal pressure	Pa
S	Allowable stress in the pipe material	Pa

3. RESULTS

3.1. Stirling engine data collection

The minimum temperature necessary, at the hot end, to run the IEAv's Stirling engine is 215 ºC. Therefore, the heat pipe condenser side operating temperature must be greater than 215ºC. Figure 6 shows the cooper coupling design, with its estimated wall temperature. That shows the temperature in the condenser wall must be on the order of 230ºC.

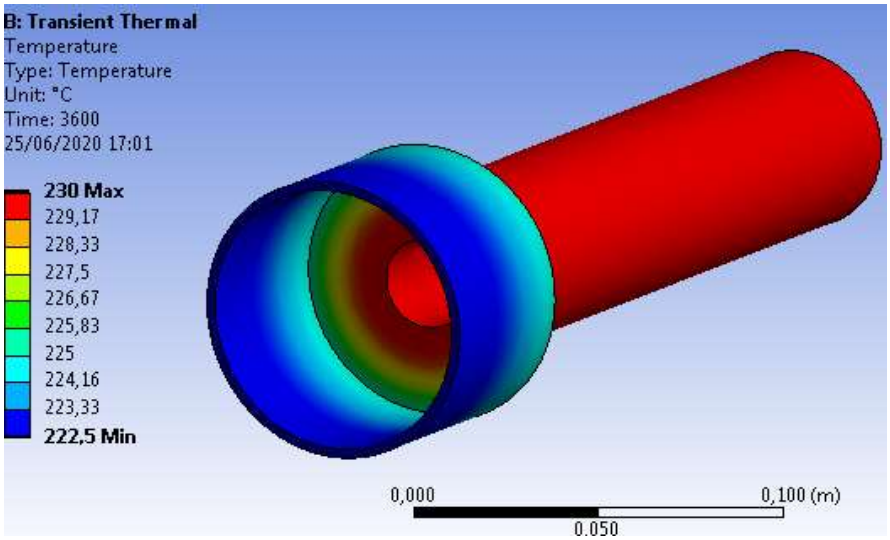

Figure 6. Distribution of temperatures at the hot end adapter surface.

3.3. Tests with heat pipe and thermosyphon

The temperatures distribution along the thermosyphon and the heat pipe test are presented in the graphs of Fig. 7 (A) and (B), respectively.

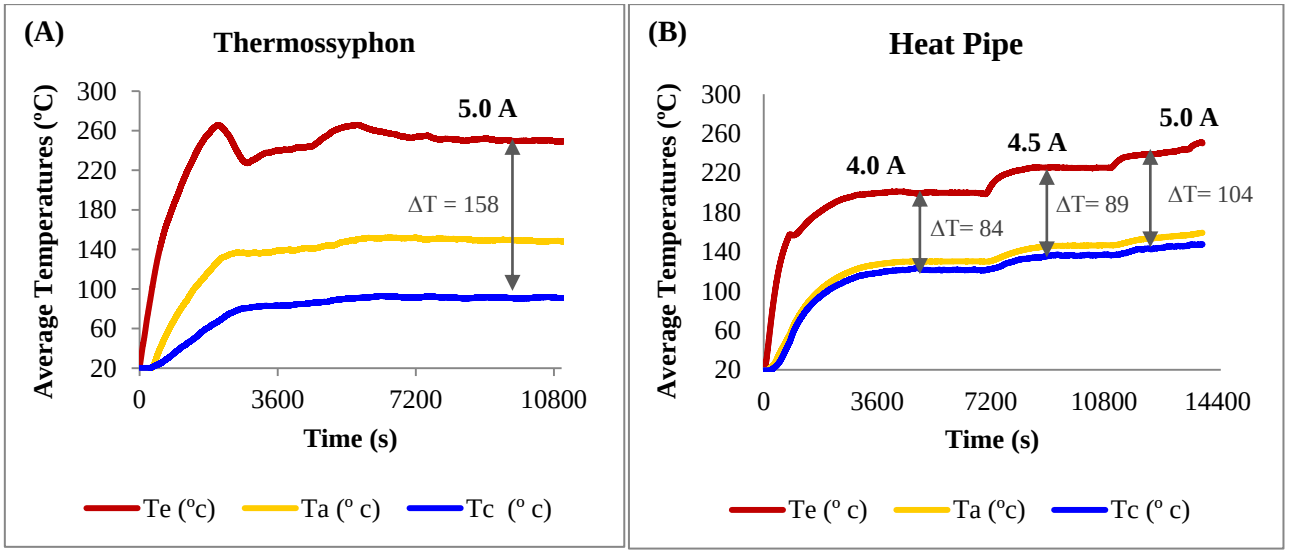

Figure 7. Distribution of average temperature in the condenser (Tc), evaporator (Te) and in the adiabatic region (Ta).

The steady state operation regime of the thermosyphon occurred at the 5.0 A applied at the thermal ribbon for heating power generation, after about 1.5 hours (5400 s). The evaporator temperature (Te) was approximately at 250 ºC ± 8.16 ºC and the condenser temperature (Tc) was at 92 ºC ± 5.54 ºC, so this produced a gradient of 158 ºC. For the (EUPHRASIO, 2019) heat pipe case, three current levels were used, respectively: 4, 4.5 and 5 A. The results of these experiments are shown in Fig 7-B. Note that the evaporator temperature rises according to the current increases, respectively: 206ºC ± 5.03 ºC, 225 ºC ± 5.54 ºC and 251 ºC ± 5.91 ºC. The temperature gradient between the evaporator and the condenser increased as the current increased, respectively: 84ºC, 89ºC and 104ºC. It is a fact that the condenser is operating at 147 ºC, which is higher than the 92 ºC from the thermosyphon. Also, none of these experiments reached the temperature of 230 ºC required for the adapter to activate the Stirling engine. Table 4 summarized the results of temperatures obtained for the experiments.

Table 4. Temperatures obtained results for the thermosyphon and heat pipe steady state operation regime.

	Thermossyphon	**Heat Pipe**		
	5.0 A	4.0 A	4.5 A	5. A
Te - Evaporator temperature	250 ºC ± 8.16 ºC	206ºC ± 5.03 ºC	225 ºC ± 5.54 ºC	251 ºC ± 5.91 ºC
Tc- Condenser temperature	92 ºC ± 5.54 ºC	122ºC ± 2.37 ºC	136ºC ± 3.5 ºC	147ºC ± 4.91 ºC
ΔT - Temperature gradient	158 ºC	84 ºC	89 ºC	104 ºC

To improve the insulation and reduce the temperature drop in the heat pipe, an aluminum thin sheet was attached to the condenser region. After that, a drop in the temperature gradient was observed (ΔT = 55 ºC), as it can be seen in the graph of Fig. 8. The evaporator temperature (Te) was 285 ºC ± 6.76 ºC and the condenser temperature (Tc) was 230 ºC ± 1.8 ºC. The explanation for this drop in temperature gradient is that the aluminum sheet has two sides: one reflective and one matte. The reflective and smooth side of the aluminum sheet in contact with the condenser wall reflects the heat and thus, heat waves reach the surface of the pipe and are absorbed back by the condenser wall, increasing the temperature in the condenser.

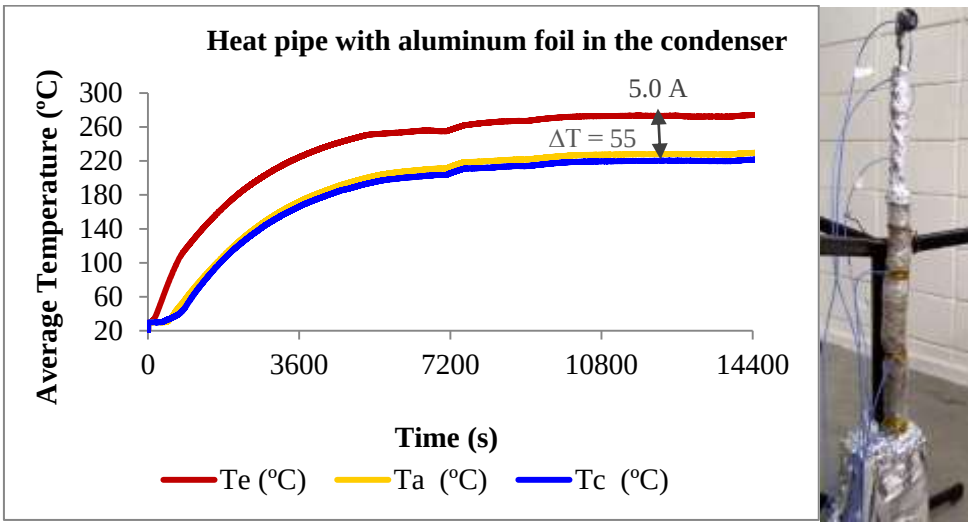

Figure 8. Distribution of average temperature in the condenser (Tc), evaporator (Te) and in the adiabatic region (Ta).

The graph of Fig. 9 shows the values of the vapor pressure inside the pipe. The highest internal pressure reached around 4.68 MPa. This pressure is less than the maximum internal pressure of the pipe that can be supported by the material (32.23 MPa). The pipe will operate without damage and accidents in this temperature range.

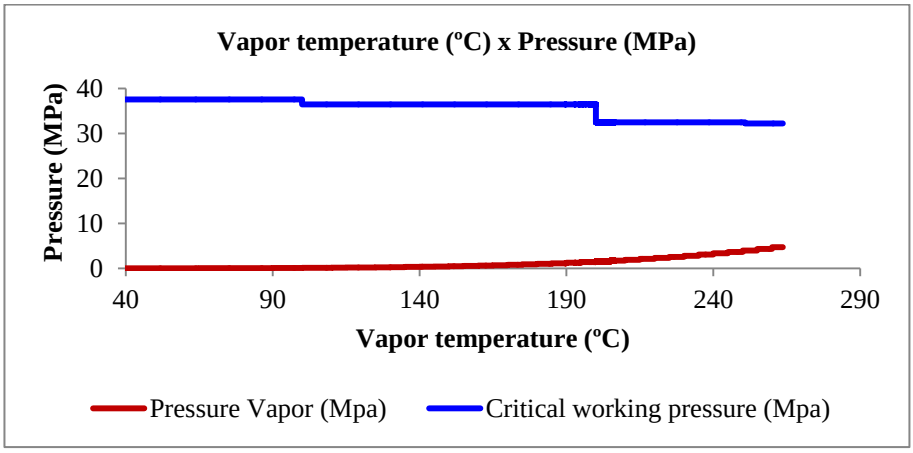

Figure 9. Characterization of the heat pipe: internal pressures inside the pipe.

The characterization of the heat pipe was performed using the test data with the aluminum sheet at the external surface of the condenser. The operating limits shown in the Tab. 5 represent the maximum power at which the heat pipe can operate, above these operating limit values the pipe fails. The lowest operating limits of the temperature range of

interest (250 - 285 ºC) are the boiling (4.4 kW) and entrainment (5.3 kW) limits. The boiling limit occurs when the radial heat flow applied to the heat pipe evaporator is very high. The entrainment limit occurs when the vapor space is not large enough for the specified power requirement. If the boiling or entrainment limits are reached, drying of the heat pipe will occur. It is observed that the sonic and viscous power value limit is very high. Viscous limit occurs when the operating temperature is below the recommended temperature and sonic limit occurs when the vapor flow reaches sonic speed as it leaves the evaporator, resulting in large temperature gradient. In the operating range of interest, the maximum power transferred by the heat pipe is 32 W. Thus, with these conditions of the carried out tests, the heat pipe did not approach any operating limits.

Table 5. Characterization of the heat pipe: Power transports limit (kW).

Vapor Temperature (ºC)	Sonic (kW)	Boiling (kW)	Entrainment (kW)	Viscous (kW)	Project (kW)
50	8.9	4.2	4.1	5.90×10^{3}	0.025
100	53.0	8.3	9.0	5.20×10^{5}	0.029
150	100.0	4.4	10.0	9.00×10^{6}	0.031
200	88.0	4.9	8.4	2.80×10^{7}	0.029
285	71.0	4.4	5.3	9.10×10^{7}	0.032

Figure 10 (A) shows the transferred power (W) in the pipe in relation to the vapor temperature. Note that the power does not show a linear behavior, however it is observed that the power increases with the increasing temperature. This increase in power is related to the decrease in total resistance shown in Fig. 10 (B). This is because the global thermal resistance of a heat pipe represents the difficulty that the device has in transporting heat. Thus, the lower the resistance, the less difficult the system will have in transporting heat and therefore the greater the thermal power (W) will be.

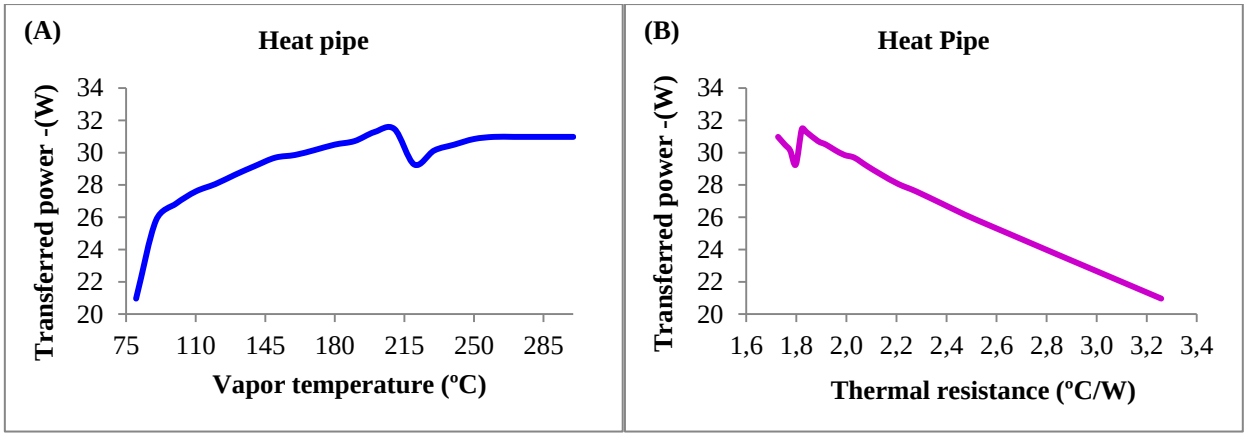

Figure 10. In (A) vapor temperature versus transferred power and (B) thermal resistance versus transferred power.

Table 6 shows the correlation between vapor temperature and Reynolds vapor number. Note that the higher the vapor temperature, the greater is the Reynolds number. For the temperature range required to carry the heat to run the Stirling engine, the vapor Reynolds number is equal to 7603.

Table 6. Correlation between Reynolds number and vapor temperature.

Tv (ºc)	Te (º C)	Tc (º C)	ΔT	Reynolds Vapor	Flow
50	108	41	67	920	Laminar
100	157	96	61	2023	Laminar
150	203	145	59	4008	Turbulent
200	245	190	55	5044	Turbulent
250	285	230	55	7603	Turbulent

Reynolds number is directly related to the speed and indirectly to the dynamic viscosity of the fluid inside the tube. The speed of the fluid increases and its viscosity decreases with the increasing temperature, so, with this, the number of Reynolds also increases. By increasing the number of Reynolds, the flow becomes turbulent, substantially increasing the heat transfer process (ZOHURI, 2016). The Reynolds number will influence the internal pressure inside the tube, the vapor friction coefficients and, consequently, the capillary pressure will be responsible for pumping the working

fluid. The tests carried out in this paper were done with the pipes mounted perpendicularly to the floor. Thus, gravity influences the performance of the tube and the capillary limit is not important in this condition. However, new future tests will be performed with the pipe in the horizon position to reduce gravity effects.

4. CONCLUSIONS

This paper presented an experimental research of the operating parameters of a thermosyphon and a 100 mesh heat pipe existing in the IEAv for application in the transport of heat from a thermal source to the hot end of the Stirling engine. It was possible to collect the temperatures of the Stirling engine in operation and with these temperatures design an adapter copper piece between the hot end of the Stirling engine and the condenser section of the heat pipe or thermosyphon. With these data it was possible to determine the temperature of the pipe condenser (greater than 215ºC).

Tests with the thermosyphon showed that it was not in compliance with the design requirements, as the evaporator temperature was 250 ºC ± 8.16 ºC and condenser 92ºC ± 5.54 ºC. The tests with the 100 mesh heat pipe showed temperature values of 251 ºC ± 5.91 ºC at the evaporator and 147 ºC ± 4.91 ºC at the condenser. But when the condenser of the same pipe was cover with the aluminum sheet, the temperatures of 285 ºC ± 6.76 ºC at the evaporator and 230 ºC ± 1.8 ºC at the condenser were obtained. The Condenser temperature is sufficient to transport the heat from a thermal source to the Stirling engine. Finally, with the temperatures collected in the experiments, the characterization of the heat pipe was carried out with: calculation of critical pressures, operational limits, Reynolds number, thermal resistances and thermal power transferred. With this paper it is possible to plan/design and adapt the test conditions for the future experiments with the complete set (thermal source + heat pipe + Stirling engine).

5. ACKNOWLEDGEMENTS

This study was financed in part by the Coordenação de Aperfeiçoamento de Pessoal de Nível Superior - Brasil (CAPES) - Finance Code 001. Acknowledgments are provided to the TERRA project, IEAv and Felipe Euphrásio.

6. REFERENCES

Euphrásio Pacheco, F., 2016. *Procedimentos para a construção e análise de funcionamento de um Termossifão*. Trabalho de conclusão de curso, Faculdade de Tecnologia São Francisco, Jacareí, Brasil.

Euphrásio Pacheco, F., 2019. *Desenvolvimento, construção e análise de funcionamento de tubos de calor.* Dissertação de mestrado em Ciências e Tecnologias Espaciais, Instituto Tecnológico de Aeronáutica, São José dos Campos, Brasil.

ESDU 81038., 2005. *Heat Pipes Performance of Two-Phase Closed Thermosyphons*. ESDU International plc, London.

Holman, J.P., 2011.*Experimental methods for engineers*, McGraw-Hill, Series in Mechanical Engineering, New York, USA.

Krambeck, L., 2016. *Thermal performance experimental study of copper powder sintered capillary structures in heat pipes.* Dissertation (Master in Mechanical Engineering), Federal University of Technology, Ponta Grossa, Brazil.

Lee, K. L., Tarau, C. and Anderson, W.G., 2018. " Titanium water heat pipes for space fission power cooling". In *Nuclear and Emerging Technologies for Space - ANS NETS.* Las Vegas, United States.

Reay, D. A.; Kew, P. A., 2006. *Heat pipes: theory, design and applications.* Elsevier's Science & Technology, Oxford, 5th edition.

Santos, A. C., Guimarães, L. N. F., Leite, V. S. F. O. and Theodoro, R., 2019. "Development of a free piston stirling engine". In *International Nuclear Atlantic Conference - INAC 2019*. Santos, Brazil.

Zohuri, B., 2016. *Heat Pipe Design and Technology. Modern Applications for practical thermal management.* Springer Publishing company, New York, 2nd edition.

7. RESPONSIBILITY NOTICE

The authors are the only responsible for the printed material included in this paper.